Characterization of MSY Nanodiamonds as a Nanoparticulate Adjuvant for RiVax Vaccine

By

Allison J. Brachtenbach

Submitted to the graduate degree program in Bioengineering and the Graduate Faculty of the University of Kansas in partial fulfillment of the requirements for the degree of Master of Science.

_____

Chairperson: Dr. M. Laird Forrest

_____

Dr. Russ Middaugh

_____

Dr. Brandon Dekosky

Date Defended: 12/5/19

The Thesis Committee for Allison J. Brachtenbach certifies that this is the approved version of the following thesis:

Characterization of MSY Nanodiamonds as a Nanoparticulate Adjuvant for RiVax Vaccine

_____

Chairperson: Dr. M. Laird Forrest

Date Approved: December 5, 2019

Abstract

Vaccines are weakened or mutated versions of the pathogens that invoke an immune response through controlled and targeted delivery. Live-attenuated and inactivated vaccines invoke an immediate and protective immune response but have higher risks in a subset of patients. Subunit vaccines are an antigenic part of the pathogen that can be paired with an adjuvant to invoke an effective immune response and cause less adverse reactions. Adjuvants are made of a wide variety of materials that aid in antigenic expression in the body, in hopes of providing protection.

Nanodiamonds have a 3D carbon structure that has highly tailorable surface chemistry to provide customization for interaction of antigens that would mimic an effect similar to a virus-like particle. Here, the synthesis of modified nanodiamonds is further developed by chemical modifications into three derivatives: oxidized, acidified, and amine modified nanodiamonds. Each derivative was compositionally and morphologically characterized to understand their stability and binding capacity. The unmodified nanodiamonds were selected to be further characterized but with a vaccine called RiVax. RiVax is a mutated ricin protein that prevents ricin toxicity for up to four months, but greater longevity and immunity is desired. In *in vivo* release studies, RiVax adsorbed to the unmodified nanodiamonds had recognition of adsorbed ricin and significantly low recognition of soluble ricin, leading to a survival rate of 50% in mice. Overall, nanodiamonds did not improve the RiVax vaccine but has shown respectable alterability, which could be beneficial to other subunit vaccines.

Acknowledgements

I would first like to thank my advisor, Dr. Laird Forrest, for the opportunity and support while working in his lab. Over the past 2.5 years, I have built my fundamental concepts in drug delivery, which has allowed me to expand my horizons in ways I did not think possible. I would also like to thank my thesis committee members: Dr. Brandon Dekosky and Dr. Russ Middaugh. Both of them have taught me many concepts over the past year and have always encouraged me to go after something I am passionate about.

I would especially like to thank my mentor, Dr. K. Ryan Moulder, for the immense amount of time he has dedicated to my thesis and the guidance he has provided throughout my research. I have learned a great number of techniques and concepts from him that no amount of words could ever express my gratitude. I would also like to thank all of the current and past members of the Forrest lab and Hylapharm: Mark Craven, Jordan Hunt, Peter Kleindl, Ruolin Lu, Derek Mull, Dr. Ninad Varkhede, Dr. Ti Zhang, Dr. Chad Groer, and Melanie Forrest. Thank you for all the thoughtful discussions and advice that created a nurturing, learning environment and for the hilarious conversations that made research all the more enjoyable.

To all the collaborators who have taken the time to act as additional guidance throughout my time here: Nick Larson, Dr. Nick Mantis, Dr. Yangjie Wei, Dr. Prem S. Thapa-Chetri, and Dr. Eduardo Rosa-Molinar. Thank you for spending several hours training me on equipment and going through data analysis with me. I would also like to thank the Departments of Pharmaceutical Chemistry and Bioengineering for the amazing educational experience that has allowed me to grow and learn vastly throughout my undergrad and graduate years.

Lastly, I would like to thank my friends and family including my brother, sister, parents (all four of them), grandparents, and boyfriend for all your encouragement throughout the whole

process. They have given me endless support and encouraged me throughout my whole college experience. I am extremely fortunate to have a group of people that stay throughout the roller coaster of life and that are extremely proud of my accomplishments, especially when I need the reminder to stop and enjoy them.

Table of Contents

1. Introduction

Vaccines are biological preparations that help prevent infectious diseases by activating the immune system, which have eradicated many diseases such as smallpox and rinderpest.[1] Vaccines activate the immune system through controlled presentation of modified forms or components of infectious pathogens. Early vaccines used live-attenuated or inactivated versions of pathogens, which work well in developing both an immediate response and a protective long-term immunity but pose some risk since severe reactions are sometimes observed in a subset of patients.[2] There is no vaccination that is 100% effective, and a small percentage of vaccinated individuals will get the disease; however, this percentage is insignificant compared to individuals who are not vaccinated.

Some vaccine approaches, such as subunit vaccines, require additional components (e.g. adjuvants) to elicit a strong response to the native pathogen. Adjuvants are materials that enhance the immune response toward a specific antigen compared to the administration of antigen alone, and this way helps provide lasting protection. Figure 1 demonstrates how an

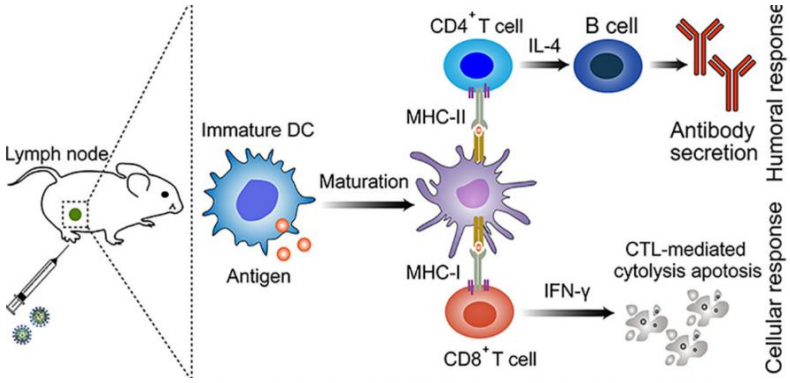

Figure 1. Targeted lymph node drug delivery to enhance a humoral and cellular response. The antigen is taken through lymphatic delivery where the antigen is presented to T- cells by an antigen presenting cell. Two paths can be taken, B-cells that help produce an antigen specific antibody to defend against extracellular pathogens (humoral response) or T-cells that defend against intracellular pathogens (cellular response). This figure is used with the permission of copyright clearance from Elsevier.

antigen, through lymphatic delivery, can cause an immune response via humoral and cellular routes of protection.[3,29]

As modern vaccine research moves forward, nanotechnology concepts are being applied to produce significant progress through improved delivery and immunogenicity.[4] Nanotechnology is the study of synthetic and organic materials on a scale of less than 100 nanometers (nm), and the fabrication of new materials that exhibit unique properties not found in their bulk equivalents. Various applications of nanotechnology exist in medicine, electronics, environmental studies, and consumer goods. In medicine, nanotechnology has been widely applied as a form of drug delivery due to targeted specificity and tailorability.[5, 6] Of note, investigations of nanoparticles has involved their versatility and applicability towards poorly water-soluble drug delivery, therapeutic co-delivery modalities, improved drug bioavailability, and many other targeted drug delivery applications. The development of nanoparticles as a protein delivery platform is an attractive approach for implementing subunit vaccines. Nanoparticles can have similar dimensions to viruses and have the potential to emulate some properties of live-attenuated vaccines including maintaining efficacy without the risks associated with their live-attenuated and inactivated counterparts.[7]

Nanodiamonds' chemical and structural properties make them a potential choice for establishing protection against toxic bioweapons, such as ricin. Ricin is a highly toxic, naturally produced protein comprised of two subunits; an A chain with cytotoxic effects and a B chain that binds to receptor moieties. Ricin poisoning halts protein synthesis by removing an adenine residue from the ribosomal RNA causing ribosomal production to decrease.[8] Immunization with RiVax, a modified form of the ricin subunit A, has shown some ability to provide short-term protection in murine models. An improved RiVax vaccine could protect those of high risk, such

as emergency first responders and military personnel, against ricin were it ever to be used as a biological weapon.[9]

In this study, characterization of various nanodiamond forms were explored to understand possible modifications that could be useful for various carbon-based nanoparticle applications toward vaccine adjuvency and subunit presentation. RiVax was used as a model protein antigen and a RiVax-Nanodiamond complex was compared to other vaccine delivery systems.

2. Background

2.1. Vaccination

The development of vaccines and their widespread implementation has nearly eradicated many deadly diseases such as polio, measles, mumps, and hepatitis A, preventing an estimated 4.5 billion cases and protecting more than 100 million lives.[10, 11] Vaccines elicit protective immunity against pathogens, commonly microbes and viruses, by priming the immune system with a safe amount of pathogen prior to infection. Historically, vaccines have been administered using four common modalities: live-attenuated, whole killed, subunit and conjugated.[12] Live-attenuated vaccines are a weakened version of the live pathogen and are very effective in conferring protective memory due to their nearly identical properties to those of the native pathogen. However, because these attenuated pathogens may replicate, there is a small possibility they can revert back to a pathogenic form and cause illness.[13] Whole killed vaccines are made by exposing the bacteria to high temperature or chemical stresses ultimately leading to pathogen death. These vaccines contain inactive pathogen, which produce an immune response but require multiple doses of the vaccine to reach the same protective efficacy as a live-attenuated vaccine.[14] Of note, all vaccines that are not live-attenuated require a booster; the

initial vaccination primes the immune system and protective immunity develops after subsequent doses are complete. Subunit vaccines are composed of an immunogenic portion of a pathogen, containing one or several epitopes.[13] These modalities provide safer, more stable vaccines which are more easily manufactured, but rarely induce a strong immune response when administered alone.[9, 12] To improve a subunit vaccine's protective capacity, conjugation of an adjuvant to the antigenic material creates an antigen-adjuvant delivery complex that often increases its immunogenicity.

2.2.Immune System

There are two different parts of the immune system involved in developing a protective immune response: innate and adaptive. Innate immunity is the immediate, nonspecific response that occurs when an immunogen is detected in the body.[17] Adaptive immunity is the antigen-specific response, which leads to long-lasting protective memory.[18]

When a foreign substance has breached the host's barriers (e.g. skin, mucosa), the innate immune response begins a set of mechanisms that recognize and neutralize invaders. First, the complement system, which is made up of a variety of circulating proteins, binds to specific motifs on pathogens not normally found in the body. When bound, these protein-pathogen complexes trigger general and specific mechanisms that lead to recruitment of innate immune cells. These phagocytes and granulocytes (macrophages, neutrophils, etc.) break down the pathogen into potential antigens. Antigen-presenting cells (APCs), such as macrophages and dendritic cells, begin presenting specific fragments of the antigen, such as epitopes, on their surface. During this process, innate immune cells produce and secrete cytokines— soluble

proteins that influence and enhance the immune response— to recruit and activate more immune cells, including lymphocytes.

The lymphocytes that make up the adaptive immune system can be divided into cell-mediated and humoral effector cells. The cell-mediated immune response recognizes and eliminates a cell that has an intracellular pathogen or genetic mutation, which can be recognized and cleared by $CD8^+$ cytotoxic T-cells. In the humoral response, APCs present epitopes to helper T-cells, which interact with naïve B-cells. Naïve B-cells differentiate to produce an influx of mature B-cells, which can make antibodies specific to the epitope to which cell is primed. Mature B-cells can also differentiate into plasma cells and memory B-cells. Plasma cells produce and secrete an abundance of antigen specific antibody. A small subset of B-cells differentiates into memory B-cells, which occurs more easily when a combination of cytokines and other immune activities are present. Memory B-cells circulate in the blood until the pathogen is reencountered to initiate a direct line of defense for subsequent exposures to similar protein epitopes.[21]

2.3.Adjuvant Technologies

Adjuvants help elicit a strong immune response towards antigens by engaging both the innate and adaptive immune systems. Some adjuvants used in approved clinical products or those currently being investigated in clinical trials include aluminum salts, oil emulsions, virus-like particles (VLPs), co-adjuvants, and nanoparticles.[22]

Aluminum salts are used in the majority of currently approved vaccines to enhance antibody production.[23] Aluminum based adjuvants, such as aluminum hydroxide or phosphate, were the first class of approved adjuvants used in 1926 for human vaccinations.[9, 24] The first

product approved that contained aluminum adjuvants was Aluminum salt precipitated diphtheria toxoid.[25, 26] Aluminum hydroxide gel (Alhydrogel® or Alum) and Aluminum phosphate gel (Adju-Phos®) are the two common forms of aluminum salt adjuvants used today, differing in crystallinity and surface charge.[9] Electrostatic interactions between antigens and aluminum adjuvants can create complexes that invoke an immune response. The nature of such interactions are a function of pH, ionic strength, and excipients.[27] However, such adjuvants often fail to induce a protective memory response.[24, 27]

Oil emulsions are thermodynamically unstable heterogenous liquids consisting of two immiscible phases (typically oil and water), which are usually stabilized by the pressure of a detergent. A strong immune response is elicited by oil emulsions due to electrostatic and hydrophobic interactions between the oil emulsion and antigen.[9] Successful emulsion-based adjuvant approaches used currently in humans are MF59 and AS03, which are approved for use in an influenza vaccine.[25] However, some emulsions have unfavorable effects like necrosis, and consequently formulations must be highly optimized and characterized to reduce undesirable side effects.[25]

Virus-like particles (VLPs) are adjuvants which aim to mimic the structure of a natural virus in hopes of generating a strong immune response.[30] VLPs have conformational epitopes on their surface presented in a patterned display similar to the native virus.[30] Gardasil is an approved VLP vaccine against the human papillomavirus that contains patterned recognition sequences that trigger the adaptive immune system, creating strong B-cell responses similar to the virus itself.[31] Since VLP scaffolds use self-forming recombinant proteins expressed from cell cultures, production and manufacturing can be relatively complex.[30] Epitopes also need to be relatively simple and well-defined to use in a VLP approach.[30, 32]

Co-adjuvants are used to target and enhance the immune response to improve protection for some vaccines. Two different adjuvants are used to act as a delivery system and an immune potentiator.[33] Current research using *in vitro* profiling uses a combination adjuvants— Quillaja Saponaria (QS-21) and 3-deactylated monophosphoryl lipid A (3D-MPL) — in formulations to produce stronger humoral and cellular responses in mice and humans for malaria immunity.[34] QS-21 is used as an adjuvant delivery system to maximize APC uptake, while the other 3D-MPL acts as an immune potentiator to help activate induction pathways of adaptive immunity.[35] However, having two adjuvants with different physicochemical properties creates high expense and complexity in manufacturing.[35]

Nanoparticles can be used as a delivery device that are manipulated to adsorb or conjugate drugs onto their surfaces. Nanoparticles can provide high carrier capacity, incorporation of both hydrophobic and hydrophilic substances, and the flexibility to administer by multiple routes.[36] A variety of nanoparticle materials, such as metallic, lipid, polymeric and carbon-based, have been explored in the clinic and are considered safe.[36] Like aluminum salts, aluminum nanoparticles generally lack the ability to stimulate the cytotoxic T-lymphocytes to fully defend against a viral infection.[37] Lipid nanoparticles suffer from aggregation due to unpredictable gelation, which can cause inflammation, dependent on the route of administration.[37, 38] Polymeric nanoparticles are often designed to be biodegradable, permitting a controlled release of drug to the target site dependent upon crosslinking, porosity, and molecular weight of the material.[37] However, polymeric nanoparticles tend to produce an uncontrollable biphasic release of the drug payload when no excipients are present.[37] Carbon-based nanoparticles are considered an attractive alternative due to their affordability, adaptability, and low cytotoxicity.[39]

2.4.Nanodiamonds

Nanodiamonds are made of carbon atoms with sp^3 orbitals, while graphite is composed of sp^2 hybridized carbon atoms. Sp^2 orbitals are prominent in graphene since the structure is a 2D hexagonal lattice sheet that is densely packed in layers, held together by π-π stacking.[40] Diamonds are made of tetrahedral sp^3 orbitals that create a 3D cubic structure.[40] The internal 3D structure of nanodiamonds lack free electrons within the carbon network, creating immense strength compared to graphene. However, the nanodiamond surface contains a significant number of orbital valences due to graphene that acts as a multicharged radical donor, which allows the empty orbitals to be filled by free radicals from other chemical groups.[40] [41] Depending on the intended end-application, nanodiamonds are synthesized through chemical vapor deposition, high pressure and temperature, or detonation.[42] Chemical vapor depositions create films that are applicable as biosensor coatings, high pressure and temperature (HPHT) nanodiamonds are useful for bioimaging, and detonation creates aggregates/agglomerates that are useful for drug delivery and some bioimaging.[42]

For drug delivery, the nanodiamond's surface can be easily manipulated for specific modifications.[42] Various functional groups, such as carboxylate, ketones, and aldehydes are present on the surface of nanodiamonds.[45] Currently nanodiamonds are being investigated for microbial detection, pathogen localization, biofilm modulation, growth inhibition, and as vaccine adjuvants.[46, 47] Because nanodiamonds have high surface adaptability, high stability, and low toxicity, there is an exciting potential for this material to modulate the immune system as a delivery adjuvant.[46]

2.5.Development of a Protective Ricin Vaccine

Ricin is a protein toxin produced by the castor oil plant, composed of two subunits (A and B chain) and in its purified form is classified as a category B biological weapon. The A chain enables its enzymatic toxic effect, while the subunit B chain is a receptor binding moiety that facilitates entry into cells.[48, 49] Subunit A is a glycosidase that removes an adenine residue from an exposed ribosomal RNA loop translation.[8] The enzymatic subunit cleavage efficiency is higher than the reproduction rate of ribosomes in the cell, which results in the death of the cell.[8] The subunit B chain binds to surface β-D-glucopyranoside moieties of the target cell and inserts molecules into an intercellular compartment to initiate translocation across the cell membrane.[48, 49] There are a number of occurrences throughout history of ricin as a bioweapon; for example, the assassination of Georgi Markov in 1978, ricin traces on a letter sent to President Obama in 2013, or a more recent occurrence in 2015 when Mohammed Ali was convicted of possession. The need for a vaccine is clear, especially for military personnel if ricin is ever aerosolized in wartime.[48]

RiVax is a vaccine candidate against the ricin toxin. RiVax is a shortened version of the subunit A-chain with point mutations to attenuate enzymatic activity and prevent vascular leak syndrome.[49] In phase I clinical trials, RiVax without adjuvants induced toxin neutralizing antibodies, like LE4, that lasted up to four months after the third inoculation.[51] However, an increase in longevity and magnitude of toxin neutralizing antibodies is highly desired.[51] LE4 is a monoclonal antibody that was made by injecting a mouse with RiVax, extracting B-cells from the mouse that express LE4, and fusing them with myeloma cells to create hybridoma cells.[52] The hybridoma cells were then purified and cultured to make the monoclonal antibodies, which

can be administered to a patient to help combat ricin toxicity and provide short term immunity.[52]

The RiVax vaccine has been formulated with Alhydrogel, which was found to increase toxin neutralizing antibodies 10-fold in mouse studies, creating an additional pilot clinical IB trial.[53] High titers were found in total and neutralizing antibodies in half the patients, but all volunteers experienced one or more toxicities from the vaccine, including headaches and nausea.[53] RiVax has also been formulated with alpha-galactosylceramide, another potential vaccine adjuvant, which promoted a humoral response and protection from ricin in a murine model.[54] However, there was a delayed onset of toxin-neutralizing activity and a passive antibody study was not performed to assess the elevated antibody levels correlated to alpha-galactosylceramide.[54] RiVax with an adjuvant elicits stronger toxin neutralizing antibodies, but toxicity and delayed onset are undesirable traits of current vaccination strategies.

The characterization of nanodiamonds was extensively explored in this study to understand the modification options possible on their surface. RiVax was used as a model antigen to see the overall potential of nanodiamonds as a delivery/adjuvant system. Lead candidates were applied to an *in vivo* mouse challenge model in an effort to improve upon the therapeutic profile of previous trials while maintaining protective capacity.

3. Materials and Methods

3.1. Materials

Monocrystalline synthetic diamond powder (MSY) was purchased from Microdiamant (Smithfield, PA). Nitric acid (Trace Metal Grade) and sulfuric acid (Certified ACS Plus) were purchased from Fisher Scientific (Pittsburgh, PA). Spermine (≥97%), N-hydroxysuccinimide (NHS), and 1-Ethyl-3-(3-dimethylaminopropyl)carbodiimide (EDC) were purchased from Acros Organics-Fisher Scientific (Pittsburgh, PA). Bovine Serum Albumin (BSA) and lysozyme were both purchased from Sigma-Aldrich (St. Louis, MO). RiVax recombinant ricin toxin A-chain V76M/ Y80A (rRTA) was expressed and purified by the Middaugh laboratory (University of Kansas, Lawrence, KS).[48, 49, 55]

3.2. Methods

3.2.1. Nanodiamond Surface Modification

Three different types of nanodiamonds were created via surface modification: oxidized, acidified, and amine conjugated, along with the unmodified source of material. The raw MSY monocrystalline diamond powder are hereafter referred to as unmodified nanodiamonds (uNDs).

Oxidized nanodiamonds (oNDs) were created by spreading uNDs thinly in a petri dish and placing in a muffle furnace (Fisher Scientific, Miami, OK) at 590 °C for 24 hours under ambient air.[45] Over the heating period the powder changed from dark grey to white.

Acidified nanodiamonds (aNDs) were developed by submerging the oNDs in a strong acidic bath (3:1 v/v H_2SO_4:HNO_3) at 25 mg/ml in a sealed vessel and microwaved in a Mars 5 Digestion Oven (CEM, Matthews, NC) for three hours at 350 °C. The acid solution was pipetted

off in a fume hood and the nanodiamonds were rinsed 3 times with 18 MΩ deionized water. The powder was then dried in a centrivap vacuum concentrator (Labconco, Kansas City, MO) at ambient temperature until completely dry.

The diamine nanodiamonds (dNDs) were synthesized by reacting the aNDs powder with spermine. aNDs were suspended in phosphate-buffered saline (PBS) at 1 mg/ml, which was made of 1 mM KH_2PO_4, 155 mM NaCl, and 3 mM Na_2HPO_4 in water at pH 7.4. NHS/EDC powders at a 1:1 volume ratio (8 mg/ml) were added to the aNDs suspension and mixed for 30 minutes at room temperature. Spermine suspended in PBS at pH 7.4 (50 mg/ml) was added dropwise to the aND/NHS/EDC mixture over 60 minutes while stirring. The mixture was reacted overnight, about 15 hours, at ambient temperature and then dried by centrivap vacuum concentrator at ambient temperature.

All modified nanodiamonds were stored at room temperature, sealed, and protected from light. Unless otherwise noted in subsequent procedures, prior to analysis, derivatized NDs were suspended in a later specified buffer and dispersed using a Model 500 Sonic Dismembrator (Fisher Scientific, Pittsburgh, PA) equipped with a 0.75-inch solid horn tip at 20% amplitude for 10 minutes.

3.2.2. Nanodiamond Surface Characterization

The surface characteristics of each ND derivative were assessed using x-ray photoelectron spectroscopy (XPS), zeta potential, Fourier transform infrared (FTIR) and raman spectroscopy. XPS spectras were collected using a PHI 5000 VersaProbe II (Physical Electronics, Chanhassen, MN). Dry samples were loaded using nonconductive double-sided tape and two points analyzed for surface composition. Full composition analysis was set at 20 scans

for carbon and 10 scans for oxygen and nitrogen. Measurements were collected using Smartsoft and data analyzed using Multipak (PHI version 9.6.1).

ND zeta potential and raman spectra were measured using a ZetaSizer Nano (Malvern Panalytical, Westborough, MA). Each zeta potential sample was suspended at 0.01 mg/ml in deionized water and placed in a quartz cuvette provided by the instrument vendor. The instrument was held at 25 °C and zeta potential assessed using three acquisitions of 10-100 scans each. Data was analyzed using a Smoluchowski model. Raman spectra were collected in the same instrument using three acquisitions at 25 °C in the quartz window cuvette, but with samples suspended in 10 mM KCl at 0.1 mg/ml. Background spectra was subtracted and data analyzed using Helix Analyze (Malvern version 10.0).

The surface functionalization of the ND derivatives was analyzed using an IRAffinity-1 S FTIR Spectrometer (Shimadzu, Lenexa, KS). Each dry powder sample was placed onto the ATR mount with a sapphire crystal and gently compacted using the instrument stylus to improve the signal. Each sample was run in absorbance mode and spectra collected between 500 cm^{-1} and 4000 cm^{-1} over 50 scans using IRsolution software (Shimadzu, version 1.2.0.).

3.2.3. Nanodiamond Sizing and Morphology

The particle size of the nanodiamonds were measured by dynamic light scattering (DLS). Measurements were made using a DynaPro plate reader (Wyatt, Santa Barbara, CA) and analyzed by Dynamics Software (Wyatt, version 7.8.2). Each sample was placed in a Grainer 96-well plate with a flat bottom and read in ten second acquisitions for five acquisitions.

Transmission electron microscopy (TEM) was performed with a FEI TECNAI F20 XT Field Emission Transmission Electron microscope (Fisher Scientific, Miami, OK) to analyze the

bulk chemistry of the nanodiamond derivatives. The microscope was equipped with a 200-kV electron source (Schottky field emitter) and a 0.25 nm TEM point resolution with a magnification range of 22x to 930,000x. Each nanodiamond derivative was suspended in ethanol at 1 mg/ml and 1 uL was placed onto a polymeric scaffold (Electron Microscopy Sciences, Hatfield, PA). Each sample was scanned in three separate structures created on the scaffolds to determine surface composition.

3.2.4. Antigen to Nanodiamond Binding Isotherms

The binding isotherm assays used BSA or lysozyme as model proteins to determine the protein adsorption capacity of the uND, oND, aND, and dND powders. The nanodiamonds were suspended in 10 mM KCl at pH 4 and then mixed with BSA or lysozyme (0.06 to 4.0 mg/mL) for 30 minutes at 4 °C. The mixtures were centrifuged at 20 ºC for 4 minutes at 14,000 x g, and the supernatant removed and tested for protein concentration using a Synergy|H1 Microplate reader (BioTek) at 562 nm for BSA and 280 nm for lysozyme on Gen5 software (BioTek version 3.03). Protein concentration was determined against a standard curve (protein at various concentrations). Supernatant protein concentration was taken as the unbound fraction and the remainder from total added taken as the bound fraction. Further studies utilized RiVax, which was added to nanodiamonds in 10 mM histidine, 10% (w/v) Sucrose, and 150 mM NaCl at pH 6 and UV absorption measured at 280nm. For pH-dependent binding isotherms, the same steps were taken but the buffer pH adjusted to 2, 4, 6, 8, 10, and 12.

3.2.5. Nanodiamond Bound RiVax Structural Integrity

Tryptophan fluorescence melts were used to detect microenvironment polarity variance between RiVax and RiVax adsorbed to uNDs. Spectra optic and 310 nm optic were used for lifetime spectrum on a fluorescence plate reader (Fluorescence Innovations Inc., Minneapolis, MN). Each sample was centrifuged at 20 ºC for 4 minutes at 14,000 g and resuspended in fresh buffer (10 mM histidine, 10% Sucrose, and 150 mM NaCl at pH 6) to ensure completely bound protein. Then 10 µL of each sample was placed in a single well of a Greiner 364-well black, flat bottom plate (N=6) (Sigma Aldrich, St. Louis, MO) and all samples were then covered with 2 µL of silica oil to prevent the sample evaporation at high temperatures. Scans were taken at every 1 °C from the interval of 10 °C to 90 °C using PR_v2 software (Fluorescence Innovations Inc. version 2.0).

3.2.6. Nanodiamond Bound RiVax Antigenicity

Bio-Layer Interferometry (BLI) using an Octet Red 96 Interferometer (Pall Forte Bio, San Diego, CA) was used to measure the association rate of nanodiamond bound RiVax to a neutralizing antibody. The antibody, LE4, was diluted to 5 µg/ml in kinetic buffer made of 0.02% (w/v) Tween 20, 0.2% (w/v) BSA, PBS, pH 7.4 and bound to an anti-mouse IgG Fc capture biosensor. Biosensors were regenerated using 10 mM glycine at pH 1.7 and stored per manufacturer instructions. Rivax was diluted to 31.25x the final concentration in 10 mM Histidine, 150 mM NaCl 10 % (w/v) sucrose at pH 6 or 10 mM Histidine and 10 % Sucrose at pH 6. uNDs at 2 mg/ml were then mixed with selected concentration of RiVax (50, 25, 12.5, and 6.25 mg/ml) to yield a final concentration of 50, 25, 12.5, or 6.25 nM with respect to RiVax. Samples were then incubated for 30 minutes at 4 °C after which all protein was assumed bound

based on previous binding isotherm results. After mixing, the samples were diluted to 10x the final desired concentration with the buffers mentioned above and then each sample was diluted with the kinetics buffer to the final desired concentration.

3.2.7. Nanodiamond Bound RiVax In-vivo Response

The mouse vaccination trials were conducted to evaluate the efficacy of the RiVax adsorbed to the uNDs compared to RiVax alone or formulated with other adjuvants. Since the concentration of RiVax for a mouse vaccine is low, the methodology was changed to permit complete binding of the antigen at low concentration.[48, 49] uNDs at 4 mg/ml were suspended in 10 mM histidine, 10% (w/v) sucrose, and 150 mM NaCl at pH 6, then point sonicated using the previously described conditions. RiVax stock (1.04 mg/ml) was thawed and 0.144 ml was diluted with 0.456 ml of histidine buffer for a final concentration of 0.25 mg/ml. From the RiVax working solution, 0.5 ml was added to 0.5 ml of the suspended nanodiamond solution for a final Rivax concentration of 0.125 mg/ml, which was then mixed by pipetting (5 times). The samples were stirred at ambient temperature, protected from light for 30 minutes to reach equilibrium binding. The Rivax/nanodiamond mixture was pipetted 5 times to resuspend any settled material and diluted to the injection concentration by removing 0.7 mL and adding 2.8 mL of diluent histidine buffer for a final Rivax concentration of 0.025 mg/ml. Before injection into the mice, the mixture was inverted to fully resuspend any sedimentation.

The mouse study was conducted at Wadsworth Center (Albany, NY) with female Swiss Webster mice that were 5-6 weeks in age (Taconic Labs, Hudson, NY). The vaccine was administered subcutaneously 40 and 19 days before challenge with a dose of 0.025 mg/ml of Rivax per mouse. Eleven days before the challenge, mice were bled from the lateral tail vein to

determine end point titers and neutralizing antibodies. Each mouse was challenged with ricin (10x lethal dose: ~2 ug/mouse)[48, 49] on day 0. The mice were then monitored for the next seven days for the onset of hypoglycemia. The glucose levels in the blood were determined with an ACCU-CHEK Aviva System blood glucose meter from Roche Diagnostics.[48] If the blood glucose levels dropped below 20 mg/dL, the mouse was euthanized.

The enzyme-linked immunosorbent assay (ELISA) microtiter studies were conducted at Taconic Labs (City, State) as previously described.[49, 57] Nunc Maxisorb F96 microtiter plates (Thermo Fisher Scientific, Miami, OK) were coated with ricin, (0.1 µg/well) in PBS (pH 7.4) and were incubated overnight at 4°C in a humidified chamber. The plates were washed three times with PBS-Tween 20 (PBS-T; 0.05%, v/v) and were blocked with goat serum (2%, v/v, in PBS-T) for 1 h at room temperature before being probed with mAbs or hybridoma supernatants diluted in mouse serum. For the ELISAs, horseradish peroxidase (HRP)-labeled goat anti-mouse IgG-specific polyclonal antibodies (SouthernBiotech) were used as the secondary reagents, and 3,3′,5,5′-tetramethylbenzidine (TMB; Kirkegaard & Perry Labs, Gaithersburg, MD) was used as the colorimetric detection substrate. ELISA plates were analyzed with a SpectraMax 250 spectrophotometer (Molecular Devices, Sunnyvale, CA), with Softmax Pro software (Molecular Devices version 5.2).

4. Results

4.1. Nanodiamond Surface Chemical Modification

Different chemical modifications were made to the MSY monocrystalline diamond powder to optimize loading potential of a protein antigen onto the surface of the nanodiamonds. The four nanodiamond forms investigated were unmodified (uND), oxidized (oND), acidified (aND), and diamine modified (dND). Chemical modifications on the nanodiamonds' surfaces were monitored by XPS to determine the chemical composition as demonstrated in Figure 2. The

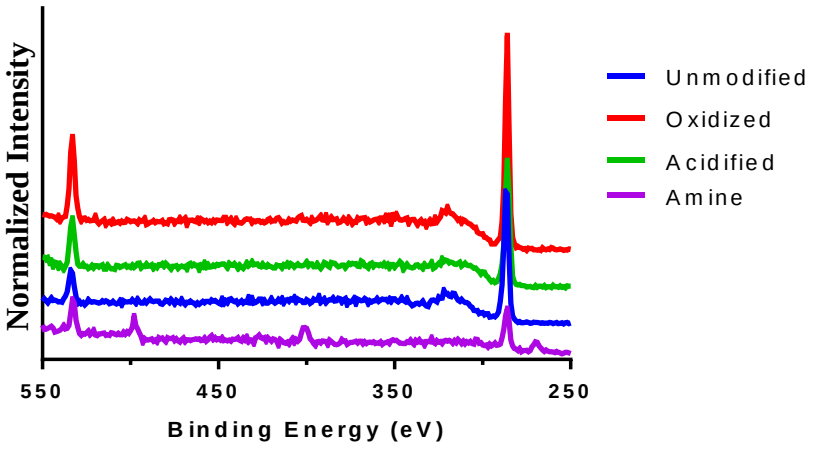

Figure 2. XPS spectrum resolution of carbon (C1) peak, oxygen (O1) peak, and nitrogen (N1) peak. The bulk surface composition for the unmodified, oxidized, acidified, and amine modified nanodiamonds were compared against each other in a stacked, overlaid view to compare the intensities correlated to the appropriate binding energy in electron volts (eV).

carbon peak (1s orbital carbons) was focused and separated into sp^2 and sp^3 hybridizations to determine the ratio of diamond carbon to graphitic carbon represented by 284.3 eV and 285.2 eV, respectively.[58, 59] The ratio of the sp^3 to sp^2 decreased with further modification. uNDs contained the highest ratio at 1.93, indicating the greatest presence of sp^3 hybridized carbons, and the dNDs contained the lowest ratio at 1.32. The oNDs had a sp^3 to sp^2 ratio of 1.75 and the aNDs ratio was 1.34. The oxygen peak around 535.5 eV had the highest intensity for the oNDs by a factor of 1.5 compared to the uNDs and aNDs, and a factor of 2 compared to the dNDs. The

nitrogen peak appeared at 401 eV and was present only on the dNDs. The additional peaks in the dNDs were the sodium and chloride atoms from the PBS buffer.

Alteration of the nanodiamonds' surface chemistry should induce changes in its surface potential indicative of various chemical functional groups. Each of the nanodiamond derivatives were suspended in 10 mM KCl at pH 4 and assessed for zeta potential. In Figure 3, changes observed in zeta potential between derivatives compared to uNDs were consistent with previously reported literature values.[45] The uNDs and aNDs had similar zeta potentials at -33.6 mV, oNDs at -25.4 mV, whereas the dNDs at 10.5 mV for the 4 hour and 9.5 mV for 21 hour

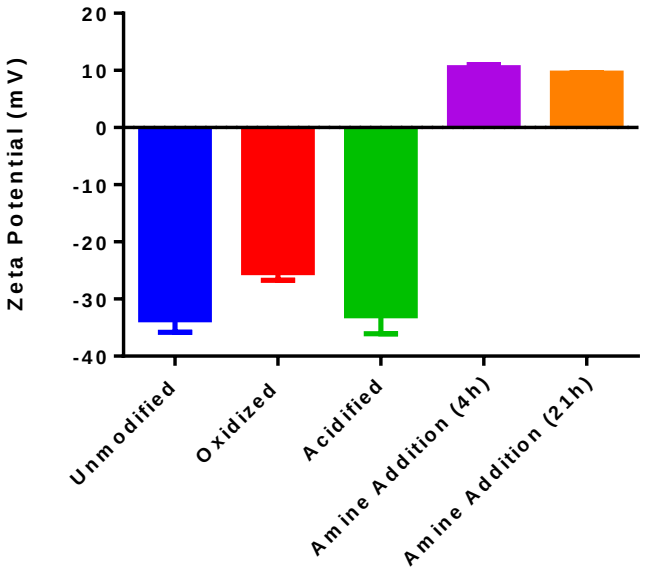

Figure 3. Surface chemical alterations were assessed by zeta potential at a concentration of 0.01 mg/ml for each nanodiamond derivative in 10 mM KCl, pH 4. Each sample (900 µL) was placed in a cuvette and scanned three times as a technical replicate.

reaction time points. The 10 mM KCl, pH 4 buffer was selected due to the positive charge affirmation due to expected surface functional groups' pKa values.[45] dNDs were measured at various times points to determine if there was any time dependent alteration in charge. No substantial changes were observed between the 4 hour and 21 hour time points.

FTIR was used to determine the change in vibrational states as the IR radiation was absorbed by particular functional groups, demonstrated in Figure 4. The spectra were noisy due to low intensity signals from the instrument, but the peaks represented in the spectrum still

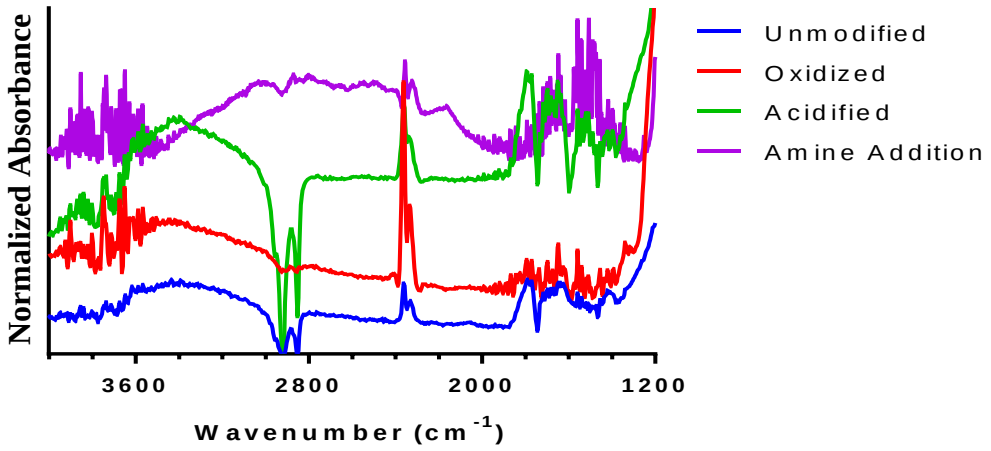

Figure 4. FTIR spectra of dry ND powders intensity were normalized and staggered to compare peak positions between derivatives.

articulate the differences between modifications. The uNDs contained a broad -OH stretching band around 3400 cm^{-1} from hydroxyls on the surface. Carboxylic anhydride stretching was present on the surface of the uNDs with C=O peak and C-O peak at 1790 cm^{-1} and 1200 cm^{-1}, respectively.[62, 63] The oNDs had an increase in C-O bonds, a decrease in -OH bonds, and a decrease in the carboxylic anhydride stretching. The aNDs had an increase in -OH stretching and an increase in the carboxylic anhydride stretching compared to uNDs. The dNDs have amide bands represented at 1665 cm^{-1}, 1550 cm^{-1}, and 1217-1317 cm^{-1}. Additional peaks confirming amines were represented between 3050-3450 cm^{-1} for NH_2 stretching/bending vibrations and NH stretching at 1630 cm^{-1}.[3, 64] The two peaks at 2800 cm^{-1} and 3000 cm^{-1} are the sp^2 and sp^3 hybridizations for CH_x atoms.

Raman spectroscopy was used to further characterize surface modifications between different physical and chemical treatments of the ND powder. The ramen spectra represented in Figure 5A depicts the carbon peak at 1330 cm^{-1} and the D-band —the disorder of the sp^2 hybrid carbons —at 1420 cm^{-1}.[45, 66] After deconvolution and integration of the Raman spectrum, the crystal lattice structure and D-band-associated peaks were assessed to quantify the difference

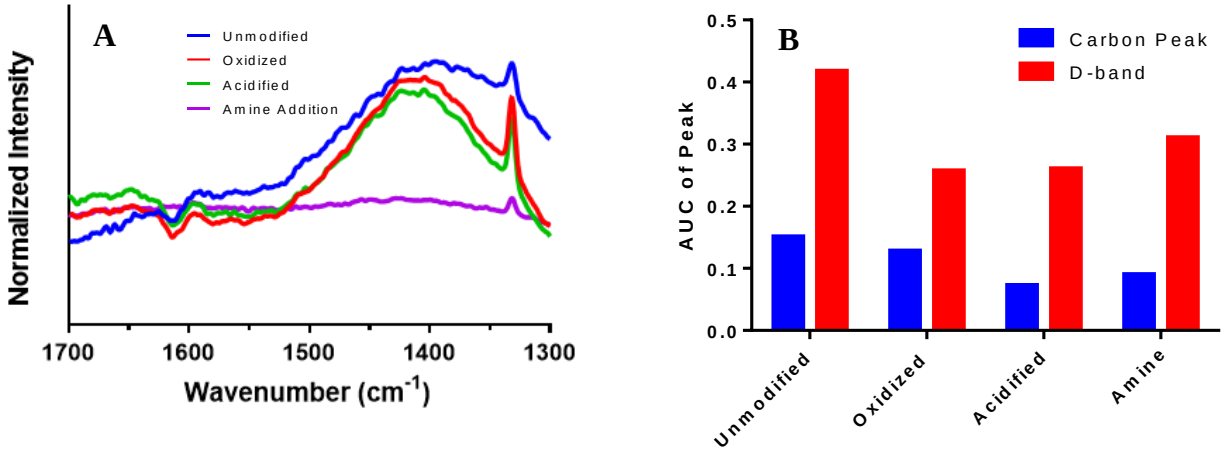

Figure 5. (A) Normalized raman spectra of nanodiamond derivatives at 0.1 mg/ml in 10 mM KCl. (B) Deconvolution and integration of 1330 cm^{-1} and 1420 cm^{-1} peaks of spectra were performed in Peakfit program.

between modifications as shown in Figure 5B. Throughout progressive modifications, the carbon peak decreased, which was attributed to the various functional groups representing a larger percentage of the overall surface. The D-band decreased in the oxidation and acidification modifications indicating a decrease in graphene on the surface.

4.2.Nanodiamond Sizing and Morphology

The hydrodynamic radius was measured using DLS to determine if any of the alterations made on the nanodiamonds altered their particle size. In Figure 6, the hydrodynamic radii of the

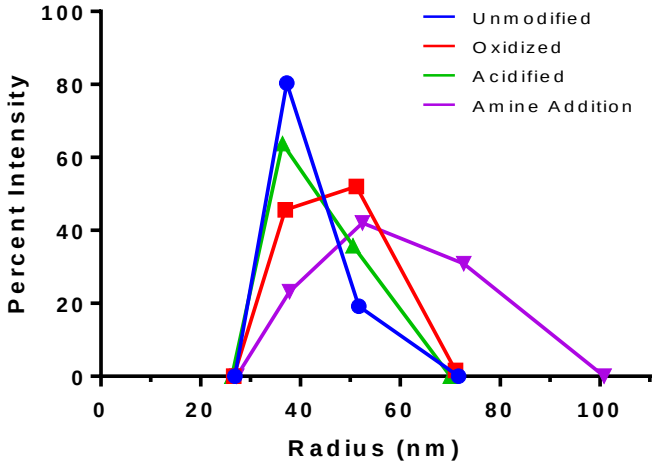

Figure 6. The hydrodynamic radius of ND derivatives verified using DLS and compared against the polystyrene microsphere standards. Measurements were made with 6 replicates of 5 acquisitions each.

derivatives were measured while suspended in 10 mM KCl at pH 4. The uNDs were measured to have a radius of 37 nm. The oNDs had an increased radius of 51 nm and the aNDs radius was similar to the uNDs at 36 nm. The dNDs had a significant increase in radius but this was deemed inconclusive due to the high sedimentation and high self-aggregation of dNDs.

TEM with an electron dispersive X-ray attachment was used to provide a compositional analysis and to observe crystalline morphology for each of the derivatives shown in Figure 7.

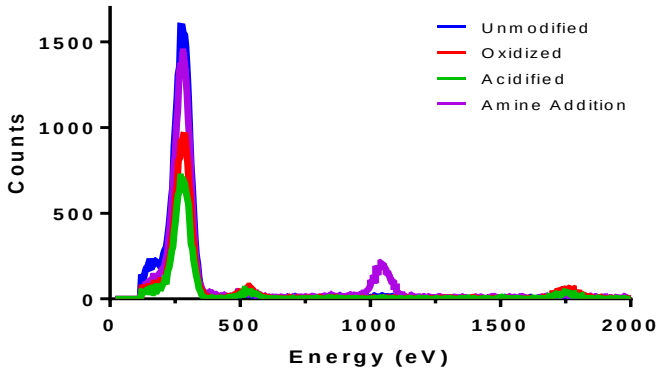

Figure 7. TEM samples were suspended in ethanol at 1mg/ml and examined within a polymeric scaffold. Three different nanodiamond clusters were examine on the scaffold and averaged to display compositional analysis.

The carbon peak at 274 eV was highest for the uNDs at 1593 counts, while the aNDs was the smallest at 713 counts. The oxygen peak represented at 532 eV and the nitrogen peak represented at 525 eV, where both slightly increased on the aNDs at 39 counts and 41 counts compared to the oNDs at 73 counts and 62 counts, respectively. Peaks present at sodium, 1044 eV, and chloride, 2612 eV, associated positions suggest residual PBS buffer remaining following the dND synthesis.

The TEM was also used to view the surface of each of the nanodiamond derivatives to determine size and the crystal lattice integrity. Granular structures were present in all images. When magnified vertical lines were present, this suggests lattice fractures in the structure.[68] The unorganized lines were either amorphous carbons or graphitically bonded glassy carbons.[69] Figures 8A and 8B are representative images used to examine the uNDs for size and crystal lattice integrity. Similar images are shown for oNDs (8C and 8D), aNDs (8E and 8F), and dNDs (8G and 8H).

Figure 8. TEM images of the nanodiamonds in clusters on the polymeric scaffold. Crystallinity and amorphous carbons were also observed in the right column to determine the amount of graphene still present.

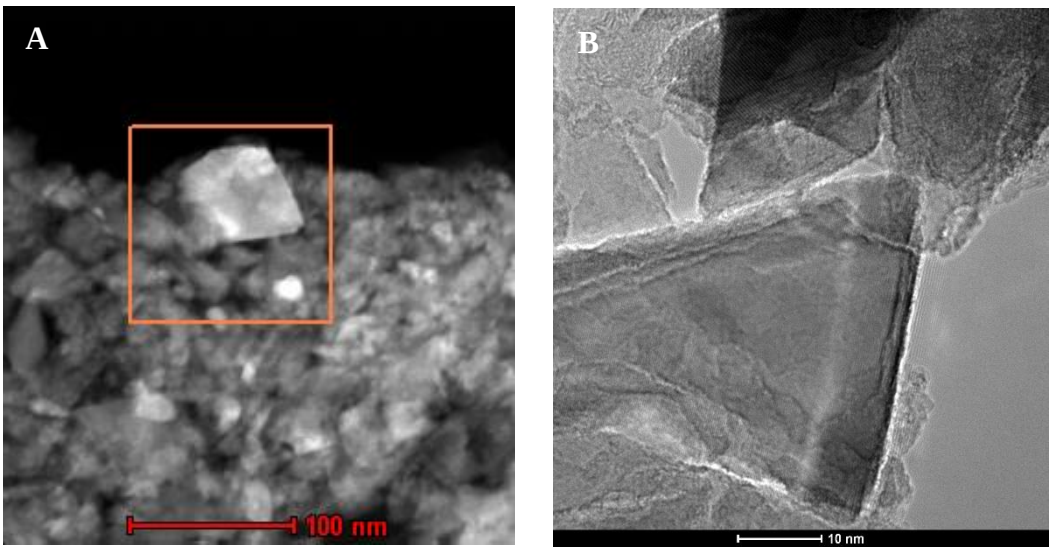

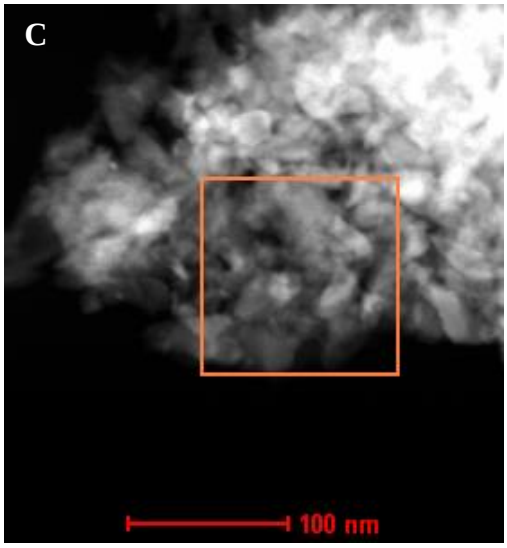
C
100 nm

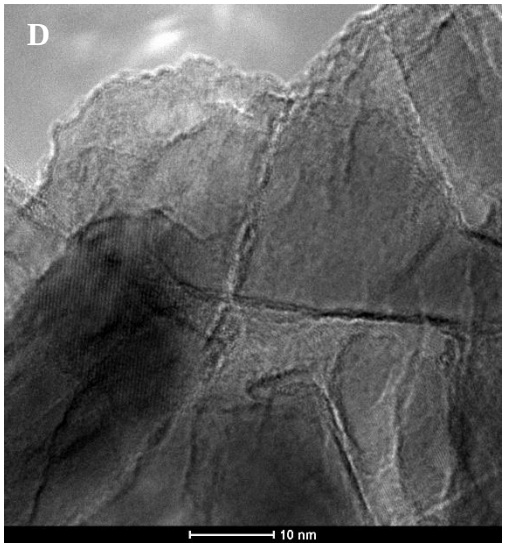
D
10 nm

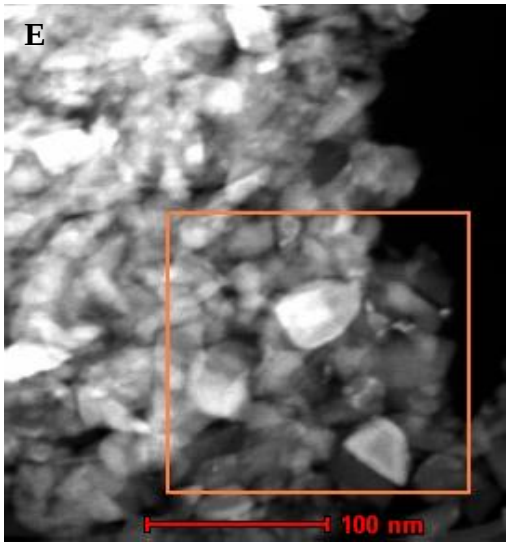
E
100 nm

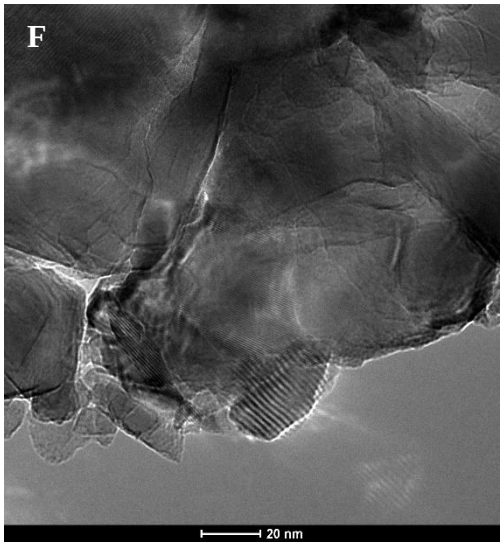
F
20 nm

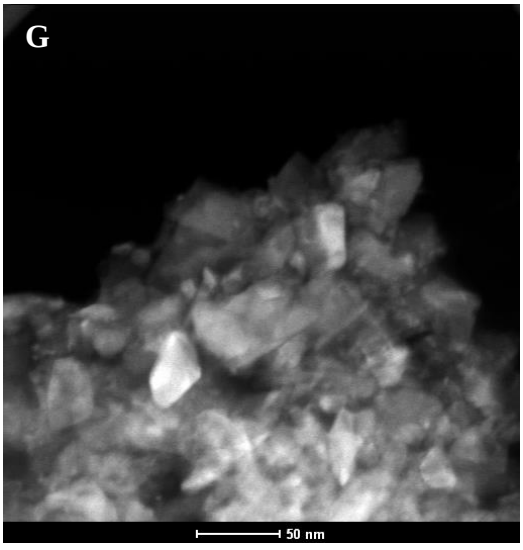
G
50 nm

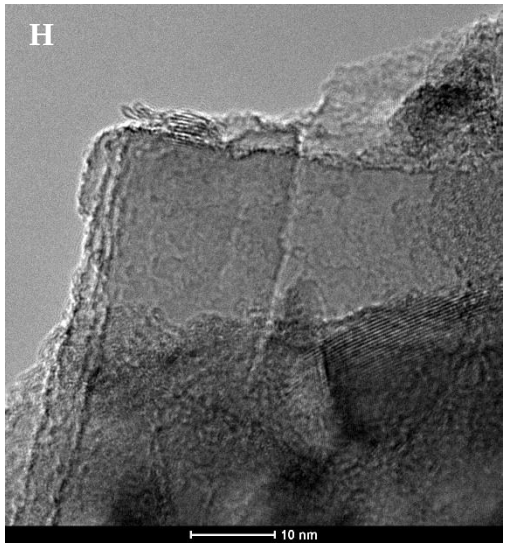
H
10 nm

4.3. Antigens on Nanodiamond associated Binding Isotherms

Two different protein antigens were selected to evaluate the loading capacity of the surface of the nanodiamond derivatives as shown in Figure 9. The model protein antigens chosen

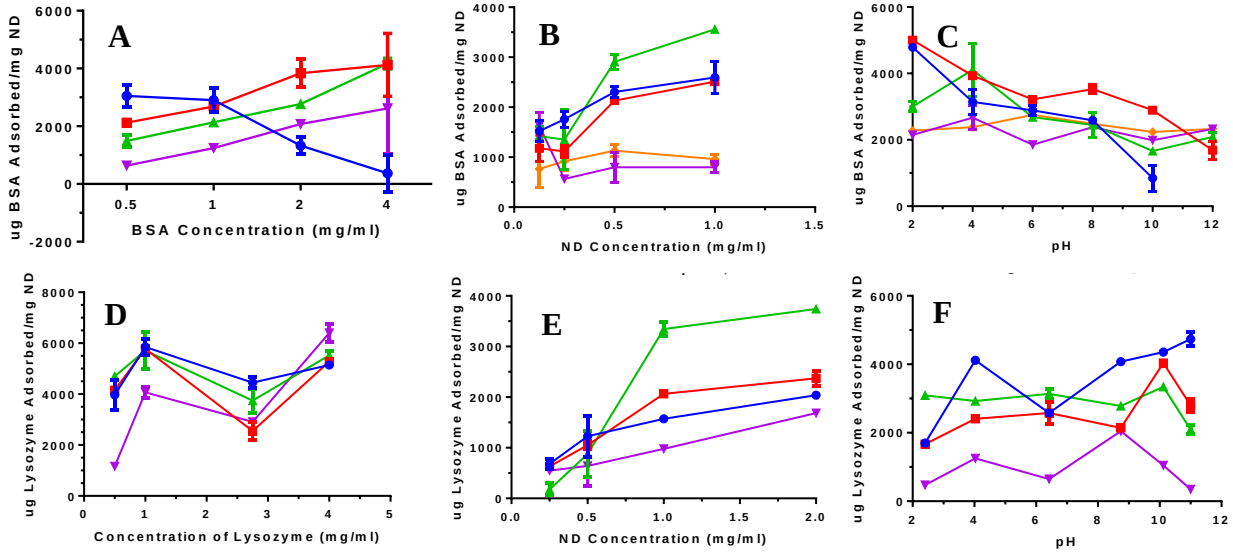

Figure 9. Binding isotherms for two model proteins, BSA (top) and lysozyme (bottom). Three separate binding isotherm variations were used varying the protein antigen concentration (left), varying the concentration of ND (middle) and varying the pH (right). Nanodiamond variants: unmodified (blue), oxidized (red), acidified (green), and amine addition (purple+ orange). Each sample mixed for 30 minutes prior to centrifugation to separate bound and unbound antigen. Three replicates were made for the concentration variations and six replicates for pH variations.

were bovine serum albumin (BSA) and lysozyme due to their opposite anionic and cationic charges at pH 7, respectively.[70] Of note, BSA isoelectric point is around 4 and Lysozyme 11. Figures 9A and 9D demonstrate the binding isotherms of BSA and Lysozyme, respectively at a constant amount (1 mg/ml) of nanodiamond. All modified nanodiamonds had no substantial change with increasing BSA concentration, except uNDs where maximized saturation of BSA occurred at 1 mg/ml. For lysozyme, no substantial difference in binding capacity was observed between the nanodiamonds except for dNDs at 0.5 mg/ml, which only bound 1/4 the capacity of other derivatives.

Figures 9B and 9E illustrates the dependence of normalized protein adsorption on ND concentration. BSA and lysozyme concentrations were kept constant at 0.5 mg/ml. The

concentration of nanodiamonds selected were 1, 0.5, 0.25, and 0.125 mg/ml for the BSA trials and 2, 1, 0.5, and 0.25 mg/ml for lysozyme. BSA had similar binding capacities for all nanodiamond derivatives except dNDs where no further BSA was adsorbed with increasing concentration of dNDs.

Figures 9C and 9F demonstrate the effects of altered pH on protein adsorption to the nanodiamond derivatives. For all anionic nanodiamonds; uNDs, oNDs, and aNDs, more BSA was adsorbed at lower pH when BSA was more cationic. dNDs did not have a significant change in binding capacity as pH became more alkaline. For lysozyme, all nanodiamonds adsorbed a constant amount of protein as the pH became more alkaline, except for uNDs. uND lysozyme adsorption increased as pH became more alkaline.

After initial binding isotherm assays, the uNDs were selected as the lead candidate for RiVax vaccine binding due to its high binding capacity, optimal size, and manufacturing simplicity for both model proteins. To understand the binding capacity of RiVax on the surface of the uNDs, various concentrations of RiVax were tested to demonstrate the saturation point of RiVax adsorbed to the nanodiamonds. The concentration of nanodiamonds were held constant at

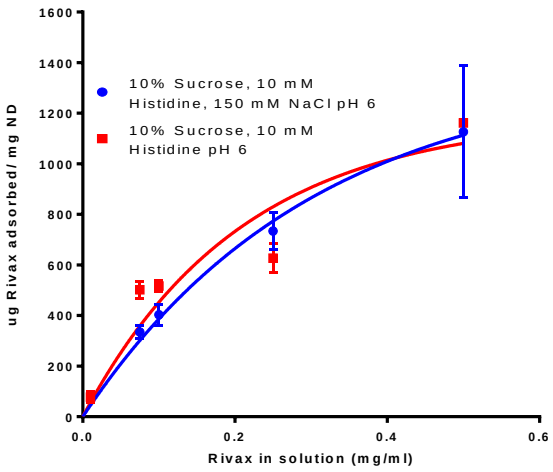

Figure 10. RiVax nanodiamond adsorption isotherms following a mixing time of 2.5 hours. The blue line (10 mM Histidine, 10% sucrose, and 150 mM NaCl) and the red line (10 mM Histidine and 10% Sucrose) at pH 6 with three replicates in each buffer. Data fit using a one-phase decay model with error bars representing ± SD.

2 mg/ml. At 0.5 mg/ml of RiVax in solution, 1380 ug of RiVax adsorbed to the surface for every miligram of uND as shown in Figure 10. Two different solutions were tested due to the extreme sedimentation of the nanodiamonds in the 10 mM Histidine, 10% Sucrose, and 150 mM NaCl buffer. Without 150 mM NaCl in the buffer, the rate of sedimentation at 4°C took 7 days longer. The salt containing buffer was selected to move forward regardless of the sedimentation risks to maintain isotonic conditions.

4.4. Nanodiamond Bound RiVax Structural Integrity

The intrinsic tryptophan fluorescence of RiVax was monitored over increasing temperatures (Figure 11) to determine the protein's melting temperature, the temperature at which its tertiary structure begins to denature. uND bound RiVax (Figure 11B) or RiVax alone (Figure 11A) in increasing concentrations (0.01 to 0.5 mg/ml) were suspended in 10 mM

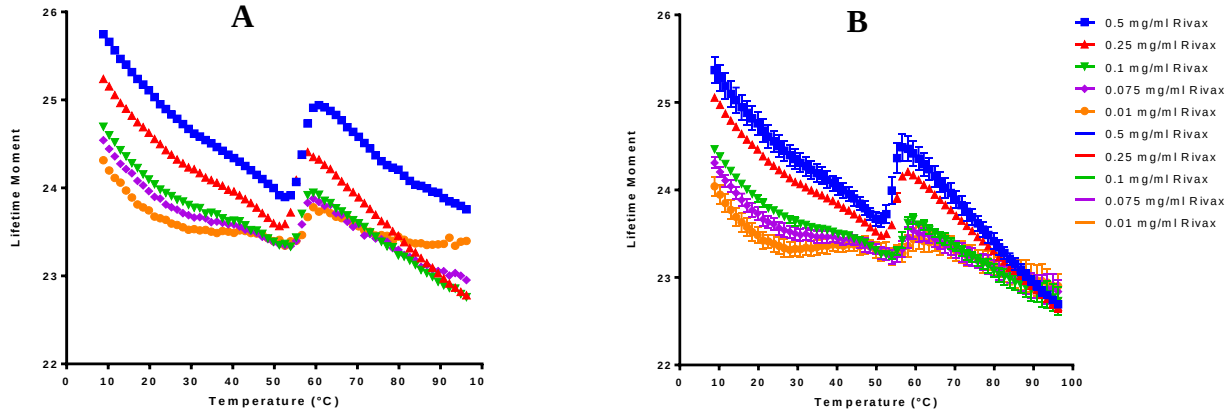

Figure 11. Intrinsic tryptophan lifetime fluorescence melts for (A) RiVax and (B) RiVax + ND. Each of the samples (n = 6) were suspended in 10 mM Histidine, 10% (w/v) Sucrose, and 150 mM NaCl at pH 6.

Histidine, 10% Sucrose, and 150 mM NaCl. Intrinsic fluorescence lifetime was measured from 10 °C to 95 °C. The melting temperature was determined by plotting the lifetime moment versus the temperature and taking the first derivative. Average melting temperature results (n=6) were 54.62 °C, 64.62 °C, 55.98 °C, 57.35 °C, and 58.71 °C for uND + RiVax in descending

concentrations and 55.98 °C, 54.62 °C, 55.98 °C, 55.98 °C, and 57.35 °C for RiVax in descending concentrations. There was a slight positive shift in the intrinsic tryptophan fluorescence with uND + RiVax, which demonstrated a difference in the tertiary structure of the protein.

FTIR was used to assess the secondary structure of RiVax when bound to the nanodaimonds surface. Following the deconvolution of the second derivative of the amide I region, structural contributions to the overall secondary structure were assessed based on previously reported spectral designations shown in Figure 12.[77] The peaks between 1600 nm and 1640 nm represent the beta sheets of the secondary structure, peaks 1650 nm to 1660 nm

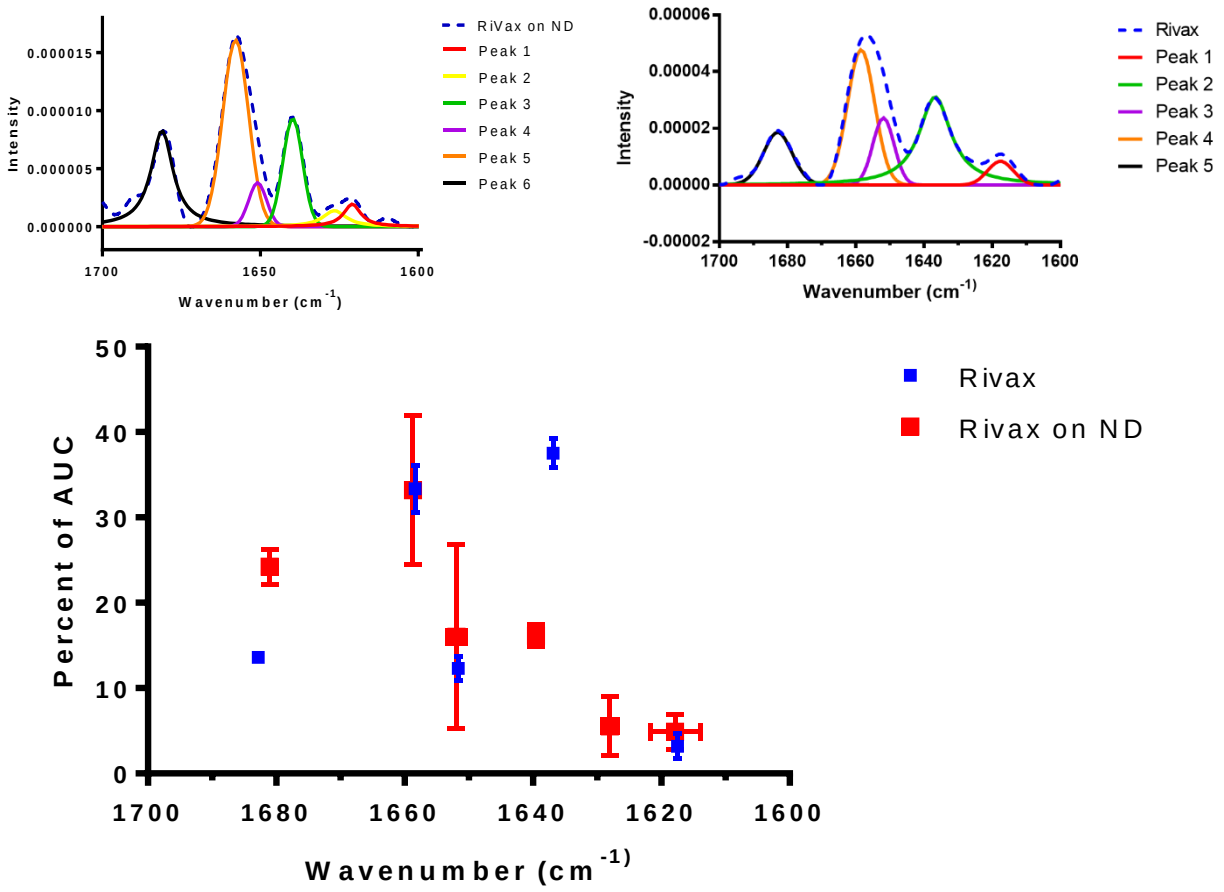

Figure 12. The secondary derivative of each FTIR spectra was deconvoluted to determine the relative contributions to the overall secondary structure for nanodiamond bound (left) and free (right) RiVax. Peak area contributions to the overall spectral area for each condition are plotted below.

represent the alpha helical structures, and peaks around 1680 nm represent the beta turns. RiVax consisted of 0.43 alpha helix, 0.43 beta sheets, and 0.14 beta turn, while RiVax on the surface of the nanodiamonds were 0.48 alpha helix, 0.27 beta sheet, and 0.25 beta turns. Secondary structure variations are present especially in the beta turn and beta sheet structures, which suggests changes in RiVax's secondary structure when adsorbed to uNDs.

4.5. Nanodiamond Bound RiVax Antigencity

Biolayer interferometry was used to quanitify antibody associaiton with uND bound RiVax. From previous studies, RiVax's neautralizing antibodies PB10, LE4, JD4,WECH, and CH1 were identified and isolated.[9] The monoclonal antibody LE4 was used for affinity comparison between RiVax and particle bound RiVax. Baseline corrected association and dissocation curves for both bound and free RiVax are seen in Figure 13. The dissocation rate was

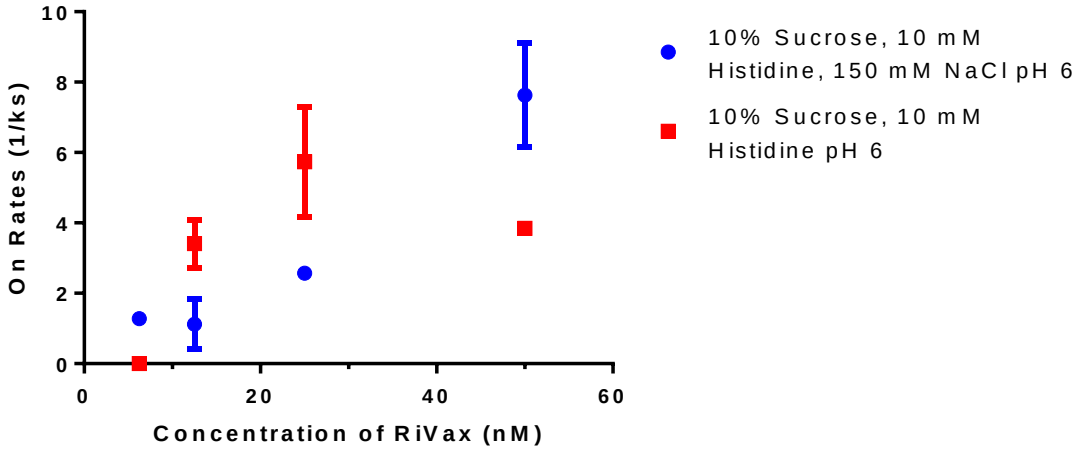

Figure 13. BLI kinetics was analyzed with LE4 at 0.05 mg/ml as the antibody and anti-mouse tips for the FAB region. Each on rate onto the tips was compared at various concentrations of RiVax and buffer conditions. The off rate was neglected due to the slow desorption off the tips.

too inconsistent to accurately measure for either condition tested likely because of the high affinity between LE4 and RiVax. With increasing concentraiton for both conditions, the on rate increased.

4.6. Nanodiamond Bound RiVax *in vivo* Response

The quanitified antibody association when RiVax bound to uNDs warrented an *in vivo* nanodiamand vaccine study using a relevant mouse model. Six mice were used for each vaccination group (RiVax and RiVax + uND). Forty days prior to challenge with soluble ricin, the two vaccines were given to each dosing group. Mice were boosted three weeks later with an equivalent does, and bled eight days priod to challenge to determine antibody titers. Mice were challenged with 2 µg ricin and monitored for 7 days. Figures 14A and 14B represent the serum dilutions tested on plates coated with ricin holotoxin in terms of absorbed light at 450 nm. uND bound Rivax immunized mouse 1, 2 and 5 sera showed low recognition of adsorbed ricin indicated by the insufficient amount of toxin-neutralizing titers. Figures 14C and 14D tested cell viability of soluble ricin, which was extremely low in all mice compared to tradition RiVax. Neturalizing end-point (EP) titers of mice dosed with RiVax + uNDs and RiVax + Alum can be viewed in Figures 14E and 14F. Stark decrease in polyclonal antibody (pAb) binding to soluble ricin versus bound ricin holotoxin are seen in the RiVax + uND immunization group.

After all mice were confirmed to have sufficient EP titers, each mouse was given a lethal dose challenge and monitored for effects. Of the six mice dosed in the RiVax + uND group, three with low EP titers died within 3 days time, while the other three survived until study termination on day 7. The three mice that survived also had signs of morbidity, such as ruffle, hunch, weakness, and tremors that improved over 7 days. No signs of morbitiy occurred on days 5-7. The mice in the RiVax, RiVax + Alum, and RiVax + AuNP immunization groups all lived and had no significant signs of morbidity except on the first day with some light ruffles and hunches observed.

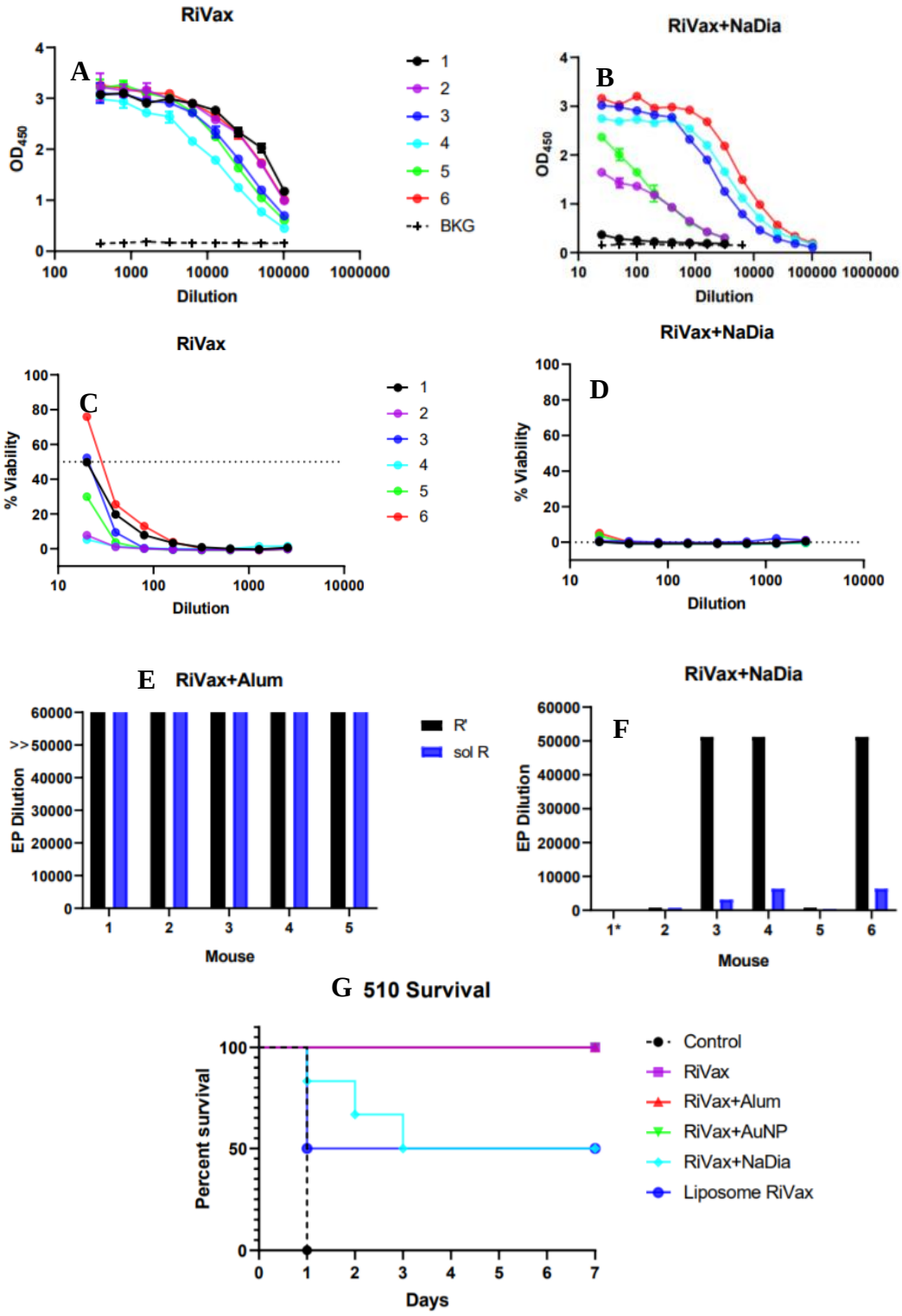

Figure 14. The ricin challenge model in 6 mice for a 2 ug/mouse dose (10x LD50), where the pre-challenge end point binding curves for ricin holotoxin were compared between (A) RiVax and (B) RiVax + uND. The serum was diluted on plates to determine the specific end point titer values for the IC50 for (C) RiVax compared to (D) RiVax + uND on the nanodiamonds. Since there were no significant amount of neutralizing antibodies produced by RiVax + uND vaccine, EP titers were determined on captured soluble ricin and non-native ricin, where (E) RiVax+Alum was used as the control to compare to the (F) nanodiamond vaccine. The Kaplan-Meier survival curve (G) was created to demonstrate the different in survival of the mice.

5. Discussion

Nanoparticulate delivery platforms that have tailorable physicochemical properties are of high interest for controlled delivery and presentation of subunit vaccine components. Nanodiamonds have easily controllable surface chemistry, which enables controlled adsorption of antigen to the surface. These complexes provide subunit presentation that mimics virus-like particles, potentially invoking an improved protective immunological response compared to subunit administration alone. In this study, nanodiamonds with varied surface chemistries were produced and characterized. Association studies with model proteins were performed to determine how these nanodiamond properties affect their binding capacity. The ricin subunit vaccine, RiVax, was used as a model subunit antigen for nanodiamond complexation in an adsorbed vaccine delivery model in hopes of improving RiVax's efficacy as a potential ricin vaccine.

Oxidative, acidic, and basic chemical modifications were explored to change functional group presentation on the nanodiamond surface in an attempt to optimize binding of a protein antigen. The specific chemical alterations were assessed by XPS, zeta potential, raman, and FTIR. Clear representation of graphitic carbons was observed on the unmodified nanodiamonds with a broad D-band in the Raman spectrum and the sp^2 peak at 3000 cm^{-1} in the FTIR spectrum. Extensive heating of the nanodiamonds results in covalent bonds between the carbon on the nanodiamond surface and ambient O_2 present in the air. This process binds oxygen to the surface of the nanodiamonds, which explains the increase in C-O groups present at 1200 cm^{-1} peak observed on the oNDs. The reduction in the D-band confirms the calorimetric change in the oxidized nanodiamonds as the graphene layers disassociate. Acidification by a strong acidic bath etches sp^2 orbitals, leading to a reduction in the D-band and a reduction in C-O bonds due to the

protonation of -COOH, -OH, -COH, etc. on the surface. Amination of the acidified nanodiamonds led to a significant N-H peak at 1100 cm^{-1} and a significant reduction in the D-band. A limitation of FTIR spectroscopy is that a significant number of peaks were not present above 2500 cm^{-1}, which could be attributed to the asymmetrical dipole moment that occurs with vibrations to produce FTIR peaks. If the bonds stretch or vibrate proportionally, the spectrum will not produce peaks due to lack of asymmetric change in the dipole moment. Raman should detect for symmetric changes, which is why we used these complimentary spectroscopy methods, but was used in this study to assess the D-band and diamond-carbon peak.

The surface charges from the zeta potential analysis for the unmodified, oxidized, and acidified nanodiamonds all support the FTIR and raman results by being highly negatively changed and can be attributed to unprotonated moities like -COOH, -OH, -COH. The amination surface charge also corresponds to the FTIR and Raman due to the positive charge from to the protonation of the amine groups.[75, 76]

The chemical compositions of the nanodiamonds were determined by the XPS analysis and confirmed the other surface chemistry characterization. A decrease in the sp^2 hybridization throughout modification was present in the spectra and the weight percent composition of the nanodiamonds agreed with FTIR. The unmodified nanodiamonds contained primarily carbon as expected since diamond is purified carbon. The oxidized nanodiamonds had a significant amount of oxygen present as expected, as covalent carbon-oxygen bonds were produced on the surface at high temperatures. The acidified nanodiamonds had no significant changes in their elemental composition compared to the oxidized nanodiamonds. Lastly, the amination nanodiamonds had a significant amount of nitrogen present on the surface due to the incorporation of the polyamine spermine.

Particle size was assessed by DLS to verify that no significant change had occurred due to modification of the nanodiamonds. The hydrodynamic radius for the unmodified nanodiamonds was 40 nm. The amine modified nanodiamonds had the widest size distribution spanning from 30 nm to 100 nm. As seen in the TEM, nanodiamonds appear in clusters and the wide size distribution observed in the data contributes to aggregation of the particles. TEM verified the crystallinity of the nanodiamonds, with vertical lines present in all images when magnified, contributing to the lattice spacing in the structure.[77] The lattice spacing confirms that sections of the nanodiamond contain diamond sp^3 hybridized carbons, while the granular structures are either amorphous carbons or graphetically bonded glassy carbons.[69] Also, the TEM compositional spectra were in agreement with the XPS compositional spectra.

Analysis of the binding capacity of the nanodiamonds to protein antigen was assessed using the model proteins BSA and lysozyme by monitoring the unbound material in solution. Initially when the nanodiamond derivatives were formulated, it was hypothesized that a cationic surface, such as the dNDs, would have the highest binding capacity since most proteins are anionic in nature (including RiVax). However, over all conditions the amine modified adsorbed the least amount of protein compared to any of the other derivatives. With the BSA binding isotherm showing increasing bind and increasing pH, no distinct changes occurred for the amine modified due to two cationic forces repelling at acidic conditions and potentially continuing repulsion in forms of an anionic charge when the solution becomes more alkaline. However, for anionic nanodiamonds such as uNDs, oNDs, and aNDs, all nanodiamonds adsorbed higher amounts of BSA (pI 4) at acidic pH because BSA becomes cationic at pH 4. With varying pH, lysozyme (pI 11) becomes less cationic at high pH. The anionic nanodiamonds should decrease in binding capacity at alkaline conditions, which does not occur. The uNDs and oNDs increase in

capacity with more basic conditions, potentially caused by non-specific binding or hydrophobic binding as lysozyme becomes less charged. No significant changes are present in the aNDs and dNDs as the pH becomes more alkaline.

The high binding capacity of the unmodified nanodiamonds lead to their selection for RiVax complexation and characterization. The unmodified nanodiamonds adsorbed 1380 µg of RiVax/mg of nanodiamond, which was almost 14 times more than the amount used in human clinical trials.[51] Nanodiamonds are efficient in adsorbing RiVax to the surface at physiological pH.

Based on intrinsic tryptophan fluorescence data, the tertiary stability of RiVax had a higher stability on the surface of the nanodiamonds than alone suggested by the 3 °C increase in melting temperature. As the protein unfolds, new tryptophan residues, which are hydrophobic become exposed. These new tryptophan residues generate increased fluorescence as shown by a large increase in the spectrum. When the buffer quenches the new residues, a steady decrease in intensity proceeds as the protein denatures and is further quenched by buffer. Since the denaturing of the protein occurred at a higher temperature, a small improved stabilization was present when bound to the nanodiamonds.

Changes to the RiVax secondary structure were observed by FTIR, with changes in alpha helices, beta sheets, and beta turns that can be attributed to the increase in melting temperature. The FTIR spectrum was observed only at the amide I peak, since the C=O stretching vibrations coupled to the N-H bonds and stretching of C-N bonds are highly sensitivity to small variations.[78] Major difference occurred in the beta sheet and beta turn structures; a 16% reduction and 11% elevation, respectively, compared to RiVax in solution. Beta turns change the direction of the polypeptide chain, which may be significant in stabilizing the formation of

tertiary interactions.[6] With a more stable secondary and tertiary structure, this could provide a longer shelf-life for the vaccine.

The affinity of RiVax + uND to LE4 antibody was assessed using BLI to quantify the rate of binding of a model anti-RiVax antibody to RiVax + uND. Of note, the dissociation was very minimal compared to the association rate, which was why the association rate, k_{on}, was used to measure affinity rather than the binding constant. As the concentration of RiVax increased the on-rate increased. In addition, non-specific binding was not present because no association was present with nanodiamond controls. A key conclusion was that when RiVax was bound to the nanodiamonds, the antigen is still recognized by antibody.

In the *in vivo* study, the holotoxin ricin was bound to a plate and coated with each mouse's serum. In the RiVax+uND dosing group, three mice had significant recognition of bound ricin, two had a moderate amount, and one had no recgonition of the toxin. Animal sera were then assesed for the amount of neutralization that occurred to soluble ricin. All antibodies produced in the RiVax+uND group had very minimal recognition to soluble ricin. Furthermore, the changes in structure of RiVax on the surface of the nanodiamond are sufficient that the Abs are not very cross-reactive to the soluble ricin. The kill curve of the mice study found that three mice died over a three-day timespan, while the RiVax alone immuniation group had no deaths. As seen in the comparision between RiVax on Alum and RiVax+uND, all mice in the Alum group had a suffient amount of recgonition and neutralization to adsorbed and soluble ricin. Since the nanodiamond subgroup had 3 mice that only had a sufficient amount of recognition to adsorbed ricin, three mice lived. To note, a group made of RiVax on liposomes also had three mice die but all mice made large amounts of adsorbed ricin and soluble ricin antibodies. Our RiVax+uND vaccine has potential but does not produce a strong enough immune repsonse to

neutralize the toxin compared to other, more commonly used adjuvent strategies. Further work will be necessary to achieve this goal.

6. Conclusion

Novel nanoparticulate vaccine platforms that are capable of providing a memory response in the body to viruses and toxins are being extensively studied. Nanodiamonds as a vaccine delivery platform have significant potential for surface manipulation and morphology that permits a wide application of possibilities. The nanodiamonds can bind antigenic material to the surface but alters the function of RiVax since the uNDs did not recognize soluble ricin. However, in the case of RiVax this is not the most suitable option as antibodies produced by the animals had insufficient recognition of soluble ricin. Overall, these results demonstrate that nanodiamonds can be used as a vaccine adjuvant but does not currently provide the best solution for a RiVax vaccine.

References

1. Klepac, P., et al., *Six challenges in the eradication of infectious diseases.* Epidemics, 2015. **10**: p. 97-101.
2. Juskewitch, J.E., C.J. Tapia, and A.J. Windebank, *Lessons from the Salk Polio Vaccine: Methods for and Risks of Rapid Translation.* Cts-Clinical and Translational Science, 2010. **3**(4): p. 182-185.
3. Petit, T. and L. Puskar, *FTIR spectroscopy of nanodiamonds: Methods and interpretation.* Diamond and Related Materials, 2018. **89**: p. 52-66.
4. Zhao, L., et al., *Nanoparticle vaccines.* Vaccine, 2014. **32**(3): p. 327-337.
5. Panyam, J. and V. Labhasetwar, *Biodegradable nanoparticles for drug and gene delivery to cells and tissue.* Advanced Drug Delivery Reviews, 2012. **64**: p. 61-71.
6. Farokhzad, O.C. and R. Langer, *Impact of Nanotechnology on Drug Delivery.* Acs Nano, 2009. **3**(1): p. 16-20.
7. Smith, D.M., J.K. Simon, and J.R. Baker, *Applications of nanotechnology for immunology (vol 13, pg 592, 2013).* Nature Reviews Immunology, 2013. **13**(9).
8. Olsnes, S. and J.V. Kozlov, *Ricin.* Toxicon, 2001. **39**(11): p. 1723-8.
9. Wei, Y.J., *Strategies to Improve the Immunogenicity of Subunit Vaccine Candidates*, in *Pharmaceutical Chemistry*. 2018, University of Kansas: Lawrence, KS.
10. Limited, H.D.S., *Ten Million Lives Saved by 1962 Breakthrough, Study Says.*, in *US Fed News Service, Including US State News*. 2017, HT Digital Streams Limited: Washington, D.C.
11. Organization, W.H., *The Power of Vaccines: still not fully utilized*, in *Ten Years in Public Heath 2007-2017*. 2017.
12. Saroja, C., P. Lakshmi, and S. Bhaskaran, *Recent trends in vaccine delivery systems: A review.* Int J Pharm Investig, 2011. **1**(2): p. 64-74.
13. Plotkin, S.A., *Vaccines: Expert Consult*, in *Vaccines: Expert Consult*. 2013, Elsevier
14. Plotkin, S.A., *Vaccines, vaccination, and vaccinology.* Journal of Infectious Diseases, 2003. **187**(9): p. 1349-1359.
15. Yan, S., W. Gu, and Z.P. Xu, *Re-considering how particle size and other properties of antigen-adjuvant complexes impact on the immune responses.* J Colloid Interface Sci, 2013. **395**: p. 1-10.
16. Zhang, X.Y. and W.Y. Lu, *Recent advances in lymphatic targeted drug delivery system for tumor metastasis.* Cancer Biol Med, 2014. **11**(4): p. 247-54.
17. Coffman, R.L., A. Sher, and R.A. Seder, *Vaccine Adjuvants: Putting Innate Immunity to Work.* Immunity, 2010. **33**(4): p. 492-503.
18. Kindt, T.J.O., Barbara A.; Goldsby, Richard A., *Kuby Immunology*. 6 ed. 2006: W.H. Freeman.
19. Medzhitov, R. and C.A. Janeway, *Innate immunity: Impact on the adaptive immune response.* Current Opinion in Immunology, 1997. **9**(1): p. 4-9.
20. Hirayama, D., T. Iida, and H. Nakase, *The Phagocytic Function of Macrophage-Enforcing Innate Immunity and Tissue Homeostasis.* International Journal of Molecular Sciences, 2018. **19**(1).
21. Parra, D., F. Takizawa, and J.O. Sunyer, *Evolution of B Cell Immunity.* Annual Review of Animal Biosciences, Vol 1, 2013. **1**: p. 65-97.

22. Aguilar, J.C. and E.G. Rodriguez, *Vaccine adjuvants revisited.* Vaccine, 2007. **25**(19): p. 3752-3762.
23. Baylor, N.W., W. Egan, and P. Richman, *Aluminum salts in vaccines - US perspective.* Vaccine, 2002. **20**: p. S18-S23.
24. Vo, H.T.M., et al., *Alum/Toll-Like Receptor 7 Adjuvant Enhances the Expansion of Memory B Cell Compartment Within the Draining Lymph Node.* Frontiers in Immunology, 2018. **9**.
25. Lee, S. and M.T. Nguyen, *Recent Advances of Vaccine Adjuvants for Infectious Diseases.* Immune Network, 2015. **15**(2): p. 51-57.
26. Lambrecht, B.N., et al., *Mechanism of action of clinically approved adjuvants.* Current Opinion in Immunology, 2009. **21**(1): p. 23-29.
27. Fox, C.B., et al., *Working together: interactions between vaccine antigens and adjuvants.* Ther Adv Vaccines, 2013. **1**(1): p. 7-20.
28. Jones, L.S., et al., *Effects of adsorption to aluminum salt adjuvants on the structure and stability of model protein antigens.* Journal of Biological Chemistry, 2005. **280**(14): p. 13406-13414.
29. Zhong, X., et al., *An aluminum adjuvant-integrated nano-MOF as antigen delivery system to induce strong humoral and cellular immune responses.* J Control Release, 2019. **300**: p. 81-92.
30. Roldao, A., et al., *Virus-like particles in vaccine development.* Expert Review of Vaccines, 2010. **9**(10): p. 1149-1176.
31. Jennings, G.T. and M.F. Bachmann, *Immunodrugs: therapeutic VLP-based vaccines for chronic diseases.* Annu Rev Pharmacol Toxicol, 2009. **49**: p. 303-26.
32. Grgacic, E.V.L. and D.A. Anderson, *Virus-like particles: Passport to immune recognition.* Methods, 2006. **40**(1): p. 60-65.
33. Mutwiri, G., et al., *Combination adjuvants: the next generation of adjuvants?* Expert Rev Vaccines, 2011. **10**(1): p. 95-107.
34. Mbow, M.L., et al., *New adjuvants for human vaccines.* Current Opinion in Immunology, 2010. **22**(3): p. 411-416.
35. Fraser, C.K., et al., *Improving vaccines by incorporating immunological coadjuvants (vol 6, pg 559, 2007).* Expert Review of Vaccines, 2007. **6**(6): p. 1022-1022.
36. Gelperina, S., et al., *The potential advantages of nanoparticle drug delivery systems in chemotherapy of tuberculosis.* American Journal of Respiratory and Critical Care Medicine, 2005. **172**(12): p. 1487-1490.
37. Sivakumar, S.M., et al., *Vaccine adjuvants - Current status and prospects on controlled release adjuvancity.* Saudi Pharmaceutical Journal, 2011. **19**(4): p. 197-206.
38. Pardeshi, C., et al., *Solid lipid based nanocarriers: an overview.* Acta Pharm, 2012. **62**(4): p. 433-72.
39. Shenderova, O.A., *Detonation Nanodiamond Particles Processing, Modification and Bioapplications*, in *Nanodiamonds*. 2010, Springer: Boston, MA. p. 79-116.
40. Georgakilas, V., et al., *Broad Family of Carbon Nanoallotropes: Classification, Chemistry, and Applications of Fullerenes, Carbon Dots, Nanotubes, Graphene, Nanodiamonds, and Combined Superstructures.* Chemical Reviews, 2015. **115**(11): p. 4744-4822.
41. Chipaux, M., et al., *Nanodiamonds and Their Applications in Cells.* Small, 2018. **14**(24).

42. Kaur, R. and I. Badea, *Nanodiamonds as novel nanomaterials for biomedical applications: drug delivery and imaging systems.* International Journal of Nanomedicine, 2013. **8**: p. 203-220.
43. Edgington, R., et al., *Functionalisation of Detonation Nanodiamond for Monodispersed, Soluble DNA-Nanodiamond Conjugates Using Mixed Silane Bead-Assisted Sonication Disintegration.* Scientific Reports, 2018. **8**.
44. Nishioka, Y. and H. Yoshino, *Lymphatic targeting with nanoparticulate system.* Adv Drug Deliv Rev, 2001. **47**(1): p. 55-64.
45. Laube, C., et al., *Defined functionality and increased luminescence of nanodiamonds for sensing and diagnostic applications by targeted high temperature reactions and electron beam irradiation.* Materials Chemistry Frontiers, 2017. **1**(12): p. 2527-2540.
46. Sangiao, E.T., A.M. Holban, and M.C. Gestal, *Applications of Nanodiamonds in the Detection and Therapy of Infectious Diseases.* Materials, 2019. **12**(10).
47. Ansari, S.A., et al., *Role of Nanodiamonds in Drug Delivery and Stem Cell Therapy.* Iran J Biotechnol, 2016. **14**(3): p. 130-141.
48. Wahome, N., et al., *Novel Ricin Subunit Antigens With Enhanced Capacity to Elicit Toxin-Neutralizing Antibody Responses in Mice.* Journal of Pharmaceutical Sciences, 2016. **105**(5): p. 1603-1613.
49. Neal, L.M., et al., *A Monoclonal Immunoglobulin G Antibody Directed against an Immunodominant Linear Epitope on the Ricin A Chain Confers Systemic and Mucosal Immunity to Ricin.* Infection and Immunity, 2010. **78**(1): p. 552-561.
50. Legler, P.M., et al., *Structure of RiVax: a recombinant ricin vaccine.* Acta Crystallographica Section D-Biological Crystallography, 2011. **67**: p. 826-830.
51. Vitetta, E.S., et al., *A pilot clinical trial of a recombinant ricin vaccine in normal humans (vol 103, pg 2268, 2006).* Proceedings of the National Academy of Sciences of the United States of America, 2006. **103**(11): p. 4328-4328.
52. Geng, X.M., et al., *Research and development of therapeutic mAbs: An analysis based on pipeline projects.* Human Vaccines & Immunotherapeutics, 2015. **11**(12): p. 2769-2776.
53. Vitetta, E.S., J.E. Smallshaw, and J. Schindler, *Pilot Phase IB Clinical Trial of an Alhydrogel-Adsorbed Recombinant Ricin Vaccine.* Clinical and Vaccine Immunology, 2012. **19**(10): p. 1697-1699.
54. Yates, J.L., E. Leadbetter, and N.J. Mantis, *Alpha-galactosylcerarnide (alpha GalCer) enhances vaccine-induced protection in a model of ricin intoxication.* Human Vaccines & Immunotherapeutics, 2018. **14**(8): p. 2053-2057.
55. Wei, Y.J., et al., *Evaluation of lumazine synthase from Bacillus anthracis as a presentation platform for polyvalent antigen display.* Protein Science, 2017. **26**(10): p. 2059-2072.
56. Kulakova, I.I., *Surface chemistry of nanodiamonds.* Physics of the Solid State, 2004. **46**(4): p. 636-643.
57. O'Hara, J.M., et al., *Folding domains within the ricin toxin A subunit as targets of protective antibodies.* Vaccine, 2010. **28**(43): p. 7035-7046.
58. Diaz, J., et al., *Separation of the sp(3) and sp(2) components in the C1s photoemission spectra of amorphous carbon films.* Physical Review B, 1996. **54**(11): p. 8064-8069.
59. Arnault, J.C., *X-ray Photoemission Spectroscopy applied to nanodiamonds: From surface chemistry to in situ reactivity.* Diamond and Related Materials, 2018. **84**: p. 157-168.

60. Bolotov, V.V., et al., *The origin of changes in the electronic structure of oriented multi-walled carbon nanotubes under the influence of pulsed ion radiation.* Nuclear Instruments & Methods in Physics Research Section B-Beam Interactions with Materials and Atoms, 2014. **337**: p. 1-6.
61. Ferro, S., M. Dal Colle, and A. De Battisti, *Chemical surface characterization of electrochemically and thermally oxidized boron-doped diamond film electrodes.* Carbon, 2005. **43**(6): p. 1191-1203.
62. Zhang, Q.W., et al., *Fluorescent PLLA-nanodiamond composites for bone tissue engineering.* Biomaterials, 2011. **32**(1): p. 87-94.
63. Dolmatov, V.Y., et al., *IR spectra of detonation nanodiamonds modified during the synthesis.* Journal of Superhard Materials, 2014. **36**(5): p. 344-357.
64. Hens, S.C., et al., *Nanodiamond bioconjugate probes and their collection by electrophoresis.* Diamond and Related Materials, 2008. **17**(11): p. 1858-1866.
65. Grill, A. and V. Patel, *Characterization of Diamond-Like Carbon by Infrared-Spectroscopy.* Applied Physics Letters, 1992. **60**(17): p. 2089-2091.
66. Alvarez-Puebla, R.A., et al., *Role of nanoparticle surface charge in surface-enhanced Raman scattering.* Journal of Physical Chemistry B, 2005. **109**(9): p. 3787-3792.
67. Mochalin, V., S. Osswald, and Y. Gogotsi, *Contribution of Functional Groups to the Raman Spectrum of Nanodiamond Powders.* Chemistry of Materials, 2009. **21**(2): p. 273-279.
68. Kumar, A., et al., *Formation of nanodiamonds at near-ambient conditions via microplasma dissociation of ethanol vapour.* Nat Commun, 2013. **4**: p. 2618.
69. Qin, L.C., et al., *TEM characterization of nanodiamond thin films.* Nanostructured Materials, 1998. **10**(4): p. 649-660.
70. Ghosh, R. and Z.F. Cui, *Fractionation of BSA and lysozyme using ultrafiltration: effect of pH and membrane pretreatment.* Journal of Membrane Science, 1998. **139**(1): p. 17-28.
71. Giammarco, J., et al., *The adsorption of tetracycline and vancomycin onto nanodiamond with controlled release.* Journal of Colloid and Interface Science, 2016. **468**: p. 253-261.
72. Girard, H.A., et al., *Surface properties of hydrogenated nanodiamonds: a chemical investigation.* Physical Chemistry Chemical Physics, 2011. **13**(24): p. 11517-11523.
73. Pan, C.P., et al., *Correlation of tryptophan fluorescence spectral shifts and lifetimes arising directly from heterogeneous environment.* J Phys Chem B, 2011. **115**(12): p. 3245-53.
74. Chen, Z.C. and A. Sadana, *An analysis of antigen-antibody binding kinetics for biosensor applications utilized as a model system: Influence of non-specific binding.* Biophysical Chemistry, 1996. **57**(2-3): p. 177-187.
75. Avdeev, M.V., et al., *On the structure of concentrated detonation nanodiamond hydrosols with a positive zeta potential: Analysis of small-angle neutron scattering.* Chemical Physics Letters, 2016. **658**: p. 58-62.
76. Schrand, A.M., S.A.C. Hens, and O.A. Shenderova, *Nanodiamond Particles: Properties and Perspectives for Bioapplications.* Critical Reviews in Solid State and Materials Sciences, 2009. **34**(1-2): p. 18-74.
77. Yang, A.S., B. Hitz, and B. Honig, *Free energy determinants of secondary structure formation .3. beta-Turns and their role in protein folding.* Journal of Molecular Biology, 1996. **259**(4): p. 873-882.

78. Stehlik, S., et al., *Size and Purity Control of HPHT Nanodiamonds down to 1 nm.* Journal of Physical Chemistry C, 2015. **119**(49): p. 27708-27720.